University of Thessaly
Department of Electrical and Computer Engineering

Compressive Sampling-based Techniques for FSK Demodulation in Space Applications

Τεχνικές Συμπιεσμένης Δειγματοληψίας για FSK Αποδιαμόρφωση σε Διαστημικές Εφαρμογές

Diploma Thesis by
Charikleia Elena

Supervisors: Assistant Professor Antonios Argyriou
Assistant Professor Athanasios Korakis

Volos, 2017

Abstract

The purpose of the present diploma thesis is the development of Compressive Sampling-based techniques for FSK signals demodulation in space communications. More precisely, is being studied the performance of a Compressive Sampling-based demodulation scheme for detection of FSK modulated signals, when they are being transmitted through the space communication channel, and have been altered due to their passage through the solar corona.

It is presented in detail all the theory and implementation procedure of the FSK modulator at the transmitter side, as well as of the Compressive Sampling-based demodulator at the receiver end of the communication system. Performance results of the proposed system have been evaluated after simulations that have been conducted in AWGN channel, as well as in real space communication channel. The results demonstrate the efficiency of the Compressive Sampling-based FSK demodulation scheme in space communications, as there is achieved a performance of low Bit Error Rate values when the signal is transmitted through the space communication link, and meets hurdles due to the hard conditions in the space environment.

Περίληψη

Ο σκοπός της παρούσας διπλωματικής εργασίας είναι η ανάπτυξη τεχνικών συμπιεσμένης δειγματοληψίας για αποδιαμόρφωση FSK σημάτων, με εφαρμογή σε συστήματα διαστημικών επικοινωνιών. Πιο συγκεκριμένα, μελετάται η απόδοση που θα έχει η βασισμένη σε μειωμένους ρυθμούς δειγματοληψίας αποδιαμόρφωση FSK μεταδιδόμενων σημάτων, τη στιγμή που αυτά μεταδίδονται μέσω του διαστημικού καναλιού και υπόκεινται σοβαρές αλλοιώσεις, εξαιτίας της διαπέρασής τους μέσω του ηλιακού στέμματος.

Παρουσιάζονται αναλυτικά το απαιτούμενο θεωρητικό υπόβαθρο για την κατανόηση του συστήματος, καθώς και η διαδικασία υλοποίησης του FSK διαμορφωτή από τη πλευρά του πομπού και του βασισμένου σε συμπιεσμένη δειγματοληψία αποδιαμορφωτή στη πλευρά του δέκτη του τηλεπικοινωνιακού συστήματος. Η αξιολόγηση των αποτελεσμάτων απόδοσης του ανωτέρω συστήματος πραγματοποιείται μέσω προσομοιώσεων που υλοποιήθηκαν σε AWGN κανάλι, καθώς και σε αληθινό κανάλι διαστημικής επικοινωνίας. Τα αποτελέσματα τεκμηριώνουν την αποτελεσματικότητα και αποδοτικότητα της εφαρμογής τεχνικών συμπιεσμένης δειγματοληψίας για αποδιαμόρφωση FSK σημάτων στις διαστημικές εφαρμογές, καθώς επιτυγχάνονται χαμηλές τιμές σφάλματος bit όταν το σήμα μεταδίδεται μέσω του διαστημικού καναλιού, σε περιόδους στις οποίες συναντά εμπόδια κατά τη μετάδοσή του λόγω των δυσμενών συνθηκών που επικρατούν στο διαστημικό περιβάλλον.

Acknowledgments

With the completion of my diploma thesis, while reaching the end of my undergraduate studies in the Department of Electrical and Computer Engineering at the University of Thessaly, I would like to thank all the people who each one in their own way contributed and helped me to get at this point.

First and foremost, I would like to express my sincere sense of gratitude to my supervisor Assistant Professor Argyriou Antonios, who gave me the chance and inspired me to work in this study. I thank him for providing me with continuous guidance and precious advice during the work of my thesis.

I would also like to thank my co-supervisor Assistant Professor Korakis Athanasios for his contribution in my thesis, as well as all the faculty members of the Department for the knowledge that I acquired in my studies.

Furthermore, I would like to express my heartfelt gratitude to my friends, for being by my side these years, for the wonderful and unforgettable moments we had together, for their encouragement and support.

Last but most important, I would like to thank my family for their unceasing encouragement, patience, and support.

Contents

Chapter 1
Introduction

Humanity’s interest in exploration of our universe is enduringly growing as technology advances. Deep space missions enable humans to investigate the unknown, the vastness of space, learn about the origins and evolution of planets, solar system, and galaxies.

During each space mission, there is a lot of important information that has to be passed between the spacecraft and the ground station. Such information may include command data, satellite's location and status of hardware, images, and scientific data, as well as information about spacecraft subsystems. In addition, any issues with the spacecraft may have to be diagnosed, repaired, or moderated during their journey. Communication links consist the solely way for data exchange, while a consistently reliable communication system secures the success of the mission.

However, communication links in deep space environment face many severe challenges. First of all, the transmitted signals weaken and being dispersed in serious degree due to the extremely long communication distance. Moreover, there are periods during in which the communication link between the Earth and Space may encounter ionospheric scintillation. These periods are called Superior Solar Conjunctions and are being mainly caused when the Sun lies between the Earth and satellite or spacecraft. As a consequence of this phenomenon, the increased intervening charged particles in the spacecraft signal links weaken the transmitted signal and obstruct the successful communication [1]. Apart from ionospheric scintillation, multipath propagation and interference affect the communication link. Significant amplitude scintillation, phase scintillation, and spectral broadening effects are produced on the carrier signal, which effects become greater as the Sun-Earth-Probe (SEP) angle decreases (Figure 1.1).

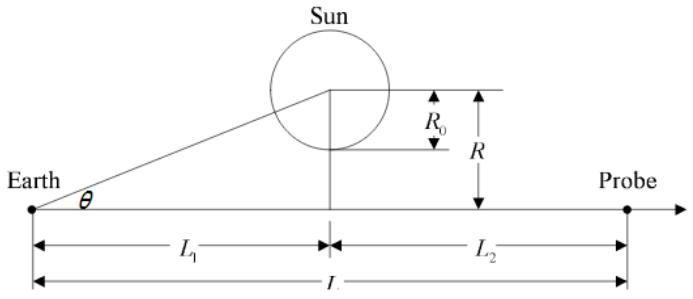

Figure 1.1: Sun-Earth-Probe Solar Conjunction geometry [3].

Signal modulation schemes that transmit data bits over frequency domain seem to provide improved data return under conditions of strong solar scintillation [2]. Frequency Shift Keying (FSK) constitutes the most conventional form of digital modulation in the high-frequency radio spectrum.

In this thesis, we present the theory and implementation of an FSK modulator and Compressive Sampling-based demodulator pair of a communication system, in order to explore their performance in space communications. FSK is the chosen modulation scheme at the transmitter side, while at the receiver Compressive Sampling (CS) techniques are applied to the demodulation process of the transmitted signals. More specifically, taking in advantage the sparsity in the frequency domain of FSK modulated signals, Compressive Sampling enables us to reduce the system complexity, power consumption and sampling rate at the receiver side. The property of FSK signals being sparse in the frequency domain, allows them also to be successfully reconstructed for the final detection of the transmitted sequence. Basis Pursuit (BP) and Orthogonal Matching Pursuit (OMP) are the two reconstruction algorithms that we tested and compared in order to observe which of these methods has as a result the most encouraging recovery performance for the compressed signals. Simulations of the proposed communication system have been conducted in Additive White Gaussian Noise (AWGN) channel, as well as in real space channel for their performance evaluation.

This thesis is structured as follows; in Chapter 2 is presented in detail all the theory on which is based the design of the FSK modulation and CS-based demodulation schemes of the communication system. More precisely, in the first part of Chapter 2 are expressed all the factors that motivated us to implement and test the performance of the FSK modulator and CS-based demodulator pair in space applications. In the following subsections of Chapter 2 is described the theory accompanied by the mathematical background, consisting essential factors for the comprehension of the implemented communication system model. In Chapter 3 are presented the experimental results for simulations of the communication system in AWGN channel and in the space channel model. Finally, in Chapter 4 is represented the conclusion and suggestions for future extensions for research in this topic.

Chapter 2
Theory of System Model

2.1 Overview of Incentives

Solar scintillation effects can be significant for deep-space communication links, especially when the Sun lies between the Earth and spaceship, meaning that the angle between the Sun, Earth and the spaceship becomes extremely small. Such effects of solar interference are expected to corrupt the data signals in varying ways or even make the communication through the space channel link impossible.

When radio waves pass through the solar corona and solar wind regions close to the Sun, strong scintillation effects influence the signal as it is being transmitted. The most significant disturbances appear at their amplitude, frequency, and phase, especially in the regions very close to the Sun [1]. Amplitude fluctuation or scintillation is designated as the short-term fading of the signal, leading to a severe drop in its strength levels. Phase scintillation is characterized by rapid carrier-phase changes, which can produce discontinuities (known as cycle slips) in a receiver's continuous phase lock on a satellite's or spaceship's signal. Another effect, spectral broadening, causes an increase in the signal's bandwidth, wherein half of the signal power resides [2].

Consequently, when the communication is feasible despite the non-favorable conditions, the received signal suffers from high rates of noise and may not include the original data information. This fact forces the receiver to attempt reacquisition of the satellite signal in order to get the desired information from the space mission.

A modulation scheme, which transmits digital information over frequency domain, is expected to be more conducive and efficient in signal estimation. A communication system based upon Frequency Shift Keying (FSK) modulation and demodulation schemes, seems to provide improved data return under conditions of strong amplitude and phase scintillation [2].

Furthermore, according to the Shannon-Nyquist sampling theorem, a band-limited signal x(t) must be uniformly sampled at least two times higher than the highest frequency presenting in the signal, to guarantee successful reconstruction at the receiver’s end. Nonetheless, when the bandwidth of the signal is too high, Analog to Digital Converters (ADCs) face a serious challenge to sample the signal and convert the latter into digital form. Moreover, it has been proved that most of the signals with large bandwidth include a small rate of information. This property of wideband signals makes them sparse in information, allowing them in that way to become compressed and represented in much fewer dimensions.

All the aforementioned factors motivated us to explore the combination of FSK modulation scheme with compressive sampling-based techniques for FSK demodulation at the receiver end, as well as their application in space communications, when the presence of challenging conditions in space environment constitute a great hurdle in signal transmission. Figure 2.1 illustrates the general form of the communication system model.

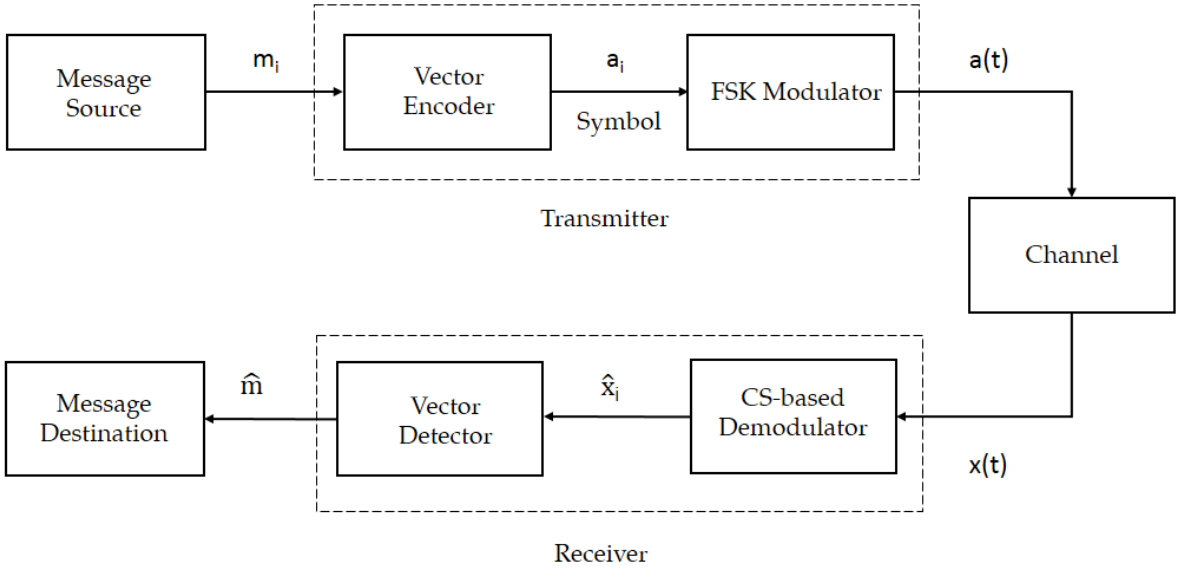

Figure 2.1: Block diagram in general form of the Communication System.

In the following subsections, is proposed in detail all the basic theory that underlies the design of the FSK modulation and CS-based demodulation schemes of the communication system.

2.2 Frequency Shift Keying (FSK) Transmitter

Binary Frequency Shift Keying (FSK) is the modulation scheme implemented at the transmitter side, in which digital information is processed and then transmitted through a pair of discrete frequency changes of a carrier wave. The frequency corresponding to the binary one is designated as the "mark" frequency, while the other referring to binary zero as the "space" frequency. Mark frequency always corresponds to the higher radio frequency. This difference in the frequency domain is what makes the binary symbols 0 and 1 be distinguished from each other when the respective one of the two sinusoidal waves is transmitted.

The FSK signals are represented by the following continuous waveforms,

$$a_0(t) = A\cos(\omega_0 t + \theta_c), \quad 0 < t \leq T \tag{2.1}$$

$$a_1(t) = A\cos(\omega_1 t + \theta_c), \quad 0 < t \leq T \tag{2.2}$$

for the binary bits 0 and 1 respectively. The signals are generated by the system illustrated in Figure 2.2.

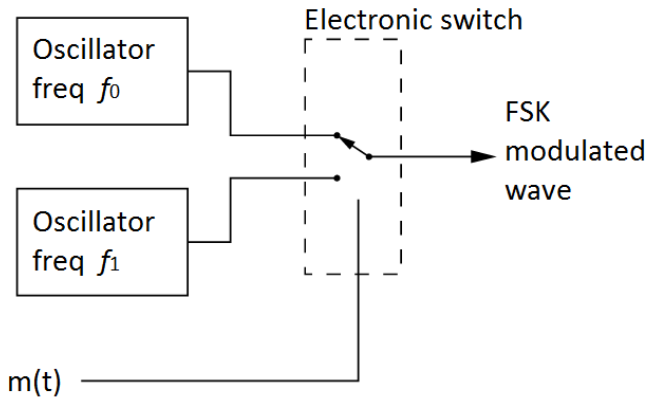

Figure 2.2: FSK transmitter system.

The two fixed-frequency oscillators produce signals of higher and lower frequency, and then they are connected to a switch along with an internal clock. The binary input sequence m(t) is applied to the transmitter so as to pick out the right frequencies according to the binary input and give as a result the FSK modulated signal that is going to be passed. The signals are transmitted coherently, implying that each FSK signal is represented by two distinct waveforms, in terms of fixed mark and space frequencies. The combination of encoding and modulation in the transmitter can be expressed as

discrete message $m_i \rightarrow a_i(t)$ continuous waveform.

In Figure 2.3 can be observed the relationship between the digital binary data input and the FSK modulated signal in the time domain that is transmitted [6].

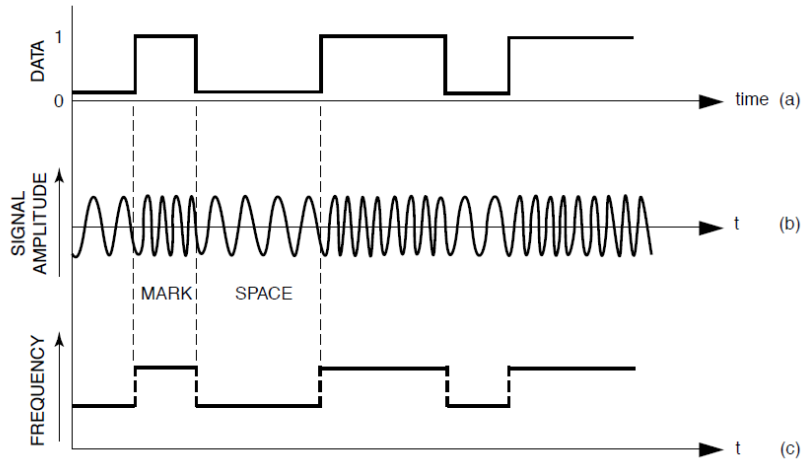

Figure 2.3: (a) Binary data in digital form, (b) FSK modulated signal, (c) frequency difference [6].

Each FSK modulated signal is specified by some key parameters which determine the transmission performance. The first parameter which refers to the minimum duration of a mark or space condition is known as "element length". Element length rates vary, depending on the kind of communication system. An alternate way to determine the element length is in terms of the keying speed, as we can see in equation (2.3).

$$\text{Keying Speed} = \frac{1}{\text{Element Length}} \tag{2.3}$$

Keying speed is computed in "bauds", in the sense of symbols per second or pulses per second and is equal to the inverse of the element length in seconds.

Frequency measurements of the FSK signal are usually stated in terms of "shift" and "center frequency". Shift is denoted as the frequency difference between the pair of frequencies f_0 and f_1, namely

$$\text{Shift} = |f_1 - f_0|. \tag{2.4}$$

The nominal center frequency is in the middle of the mark and space frequencies, defined as

$$\text{Center Frequency} = \frac{f_0 + f_1}{2}. \tag{2.5}$$

Moreover, another parameter, "deviation" is equal to the absolute value of the difference between the center frequency and the mark or space frequencies. Deviation is also equal, numerically, to one-half of the shift.

$$\text{Deviation} = \left|\frac{f_0 + f_1}{2}\right| = \frac{\text{Shift}}{2} \tag{2.6}$$

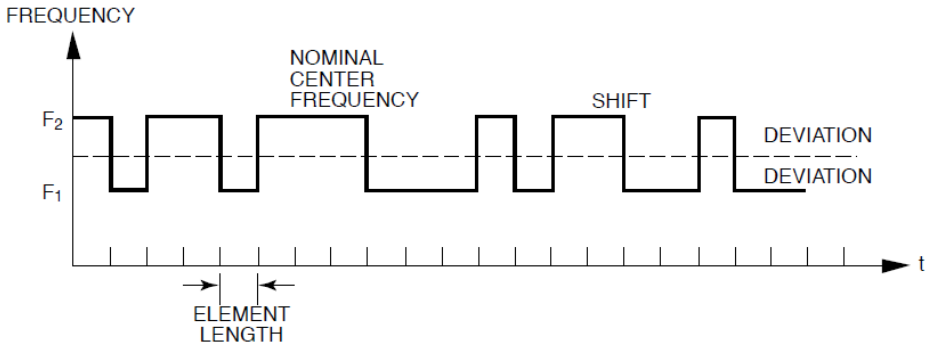

Figure 2.4: FSK parameters [6].

2.3 Signal Transmission

We consider a(t) being the FSK modulated signal that is transmitted and passes through the communication channel. If h(t) symbolizes the impulse response of the physical communications channel and n(t) the Additive White Gaussian Noise (AWGN), then the received signal x(t) can be represented as the sum of noise and convolution between the functions h(t) and a(t).

$$x(t) = h(t) * a(t) + n(t) \tag{2.7}$$

where "*" refers to the convolution operation.

The FSK signal a(t) for the k-th information symbol transmitted, is defined as,

$$a_k(t) = \sum_{n=0}^{N-1} a_{n,k}\,\delta(t - nT) \tag{2.8}$$

where N is the total number of samples per information symbol and T is the sampling period. Each sample $a_{n,k}$ is declared as

$$a_{n,k} = e^{j2\pi kn/N}. \tag{2.9}$$

Equation (2.7) can also be expressed in a matrix-vector notation like

$$\mathbf{x} = \mathbf{H}\mathbf{a} + \mathbf{n} \tag{2.10}$$

where **H** represents the channel convolution matrix and vectors **x**, **a** and **n** contain all the elements of $\mathbf{x}_n$, $\mathbf{a}_n$ and $\mathbf{n}_n$ as we can see in the expression (2.11).

$$\begin{bmatrix} x_1 \\ \vdots \\ x_n \end{bmatrix} = \begin{bmatrix} h_{1,1} & \cdots & h_{1,n} \\ \vdots & \ddots & \vdots \\ h_{n,1} & \cdots & h_{n,n} \end{bmatrix} \begin{bmatrix} a_1 \\ \vdots \\ a_n \end{bmatrix} + \begin{bmatrix} n_1 \\ \vdots \\ n_n \end{bmatrix} \tag{2.11}$$

At the receiver side, by taking advantage of the characteristic of FSK signals being sparse in frequency domain, we first compress them in order to reduce the sampling rate and the system complexity without losing important information. Sparsity also allows signals to be reconstructed efficiently and then estimated from fewer linear measurements.

2.4 Sparsity

In terms of analog signals, sparsity may mean that a signal can be expressed in terms of a suitable basis, which can transform it into a sparse representation. A sparse structure usually is discerned as it contains few large coefficients and many zero or negligibly small coefficients. FSK analog signals are such signals which can have a sparse representation in frequency domain as we can see for instance in Figure 2.5 [8].

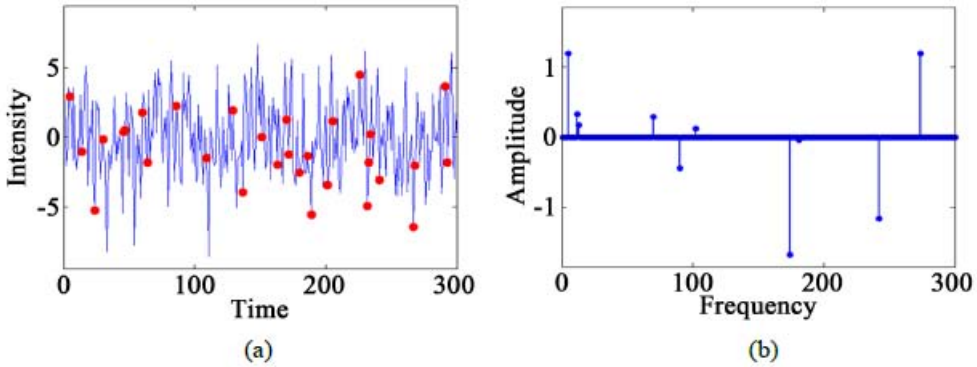

Figure 2.5: (a) Time domain signal, (b) Fourier spectrum [8].

In Figure (2.4) (a) is illustrated the intensity of an analog signal in time domain, while in Figure (2.4) (b) the different frequencies appearing in the signal are indicated by the Fourier transform $\hat{f}$.

Fourier transform refers to both the mathematical operation that associates the representation of the frequency domain to a function of time as well as the frequency domain representation itself. The Fourier transform of an integrable function $f : \mathbb{R} \rightarrow \mathbb{C}$ is defined as

$$\hat{f}(\xi) = \int_{-\infty}^{+\infty} f(x) e^{-2\pi i x \xi} dx, \tag{2.12}$$

for any real number ξ which represents frequency (with SI unit of Hertz), and for the independent variable x representing time (in seconds). The inverse Fourier transform is given by the equation;

$$f(x) = \int_{-\infty}^{+\infty} \hat{f}(\xi) e^{2\pi i x \xi} d\xi \tag{2.13}$$

for any real number x. In fact, many real-world signals have a sparse representation in a particular basis, as for instance in the time domain, frequency domain or wavelet domain.

Conventional Analog to Digital Converters (ADCs), according to the Shannon-Nyquist sampling theorem, sample analog signals at least twice the bandwidth contained in the signal. A drawback of this approach is that the bandwidth of the signal may not be a reliable representation of how much real information includes the signal, leading in this way the ADCs to sample at unnecessarily high rates. High-rate sampling is inherently more complicated than low-rate sampling. Compressive Sensing, suggests that sparsity allows a signal be represented in much fewer dimensions, leading to a reduced sampling rate and, hence, reduced use of ADCs resources.

At the receiver side of our system, Analog to Information Converter (AIC) utilizes the theory of Compressive Sensing in order to sample signals at reduced digital data rates. In this way, not only the complexity and energy consumption of ADC is reduced, but also there is focus only on the relevant information of the received signal. Compressive Sensing furthermore enables the discrete signal which has a sparse representation to be reconstructed from a small number of linear projections of that signal for the final estimation.

Consequently, the received signal vector shall be first processed by the AIC to obtain a compressed representation and be sampled at rates much lower than Nyquist. Then the signal is being reconstructed through the chosen CS reconstruction algorithms, Basis Pursuit or Orthogonal Matching Pursuit, and then the final detection rule is applied over the reconstructed signal.

In the following subsections of this chapter, is presented in detail the basic theory of compressive sampling, as well as the procedure of FSK signal compression and reconstruction that is implemented at the receiver side of the communication system.

2.5 Basic Theory of Compressive Sampling

Compressive Sampling (CS), also referred to as Compressive Sensing or Compressed Sensing, is a Digital Signal Processing technique efficiently acquiring and transforming a signal into a compressed representation, by taking only a limited set of linear measurements of the signal. In other words, Compressive Sampling can be thought of as a concept to reduce the number of measurements required to approximate a signal, without any loss of important information. Therefore, it can be processed with fewer resources and then finally reconstructed to its original form.

We consider a finite-length, one-dimensional discrete-time signal $\mathbf{x}_{N\times 1}$, which is sparse on some basis and can be viewed as a $N\times 1$ column vector in $\mathbb{R}^N$ with elements $\mathbf{x}[n]$, $n = 1, 2, \ldots, N$. If $\mathbf{\Psi}_{N\times N}$ represents the matrix containing the basis factors of $\mathbf{x}$ and $\mathbf{s}_{N\times 1}$ its respective coefficients, then $\mathbf{x}$ can be expressed as

$$\mathbf{x} = \mathbf{\Psi s} \,. \tag{2.14}$$

More specifically, the vectors $\mathbf{x}$ and $\mathbf{s}$ constitute equivalent representations of the same signal, with $\mathbf{x}$ illustrated in the time domain, and $\mathbf{s}$ in the $\mathbf{\Psi}$ domain. From the above expression, the sparsity of $\mathbf{x}$ means that it contains very few large coefficients and at the same time many zeroes or negligibly small valued coefficients. Therefore $\mathbf{x}$ is compressible, in the sense that it can be represented by M linear measurements with $M \ll N$. Let $\mathbf{\Phi}_{M\times N}$ be the transform operator $\mathbb{R}^N \rightarrow \mathbb{R}^M$, with M linear functionals as its rows. Then $\mathbf{x}$ can be transformed into a new vector representation $y \in \mathbb{R}^M$ with $M \ll N$, which is defined as

$$\mathbf{y} = \mathbf{\Phi x} \text{ or } \mathbf{y} = \mathbf{\Phi\Psi s} \tag{2.15}$$

where $\mathbf{\Phi}$ is the measurement or sensing matrix, and the basis matrix $\mathbf{\Psi}$ is the sparsity matrix. The measurement process is non-adaptive since $\mathbf{\Phi}$ is fixed and does not depend in any way on the signal $\mathbf{x}$. Sensing matrix $\mathbf{\Phi}$ plays a key role in the process of compression, as it does not only have to ensure that any K-sparse or compressible signal is not damaged by the dimensionality reduction from $\mathbf{x} \in \mathbb{R}^N$ down to $\mathbf{y} \in \mathbb{R}^M$ but should also allow for its successful reconstruction.

There are two fundamental conditions in CS under which the accurate signal recovery is feasible. The first one is the sparsity of the signal, which means that the signal has to be sparse in some basis $\mathbf{\Psi}$, as for instance in the frequency domain. Secondly, sensing matrix has to satisfy a condition known as the Restricted Isometry Property (RIP).

RIP characterizes matrices which are nearly orthonormal, at least when operating in sparse vectors. It has been found that with exponentially high probability, random Gaussian, Bernoulli, and partial Fourier matrices satisfy the RIP with a number of measurements nearly linear in the sparsity level [8].

Assuming that $\boldsymbol{\Theta} := \boldsymbol{\Phi}\boldsymbol{\Psi}$ and signal **x** is K-sparse, the formal concept of RIP states as following; Matrix $\boldsymbol{\Theta}$ acts as an approximate isometry on the set of vectors that are K-sparse, and $\boldsymbol{\Theta}$ satisfies the K-RIP if there exists the smallest number δ_K, such that

$$(1-\delta_K)\|\mathbf{s}\|_{l_2}^2 \le \|\boldsymbol{\Theta}\mathbf{s}\|_{l_2}^2 \le (1+\delta_K)\|\mathbf{s}\|_{l_2}^2 \tag{2.16}$$

where the sparsity constant δ_K depends on K, $\boldsymbol{\Phi}$ and **s**, with $\delta_K \in [0,1]$. This means that every set of K or fewer columns of $\boldsymbol{\Theta}$ is approximately orthogonal, or that $\boldsymbol{\Theta}$ is approximately orthogonal for any K-sparse vector.

Furthermore, assuming that $\mathbf{x}_i$ constitutes the elements of **x**, and the support of **x** is T = supp{i: $\mathbf{x}_i \neq 0$}, with K = |T|, if $\boldsymbol{\Theta}_T$ represents a submatrix of $\boldsymbol{\Theta}$ with columns $\theta_i : i \in T$, then RIP implies that the eigenvalues of $\boldsymbol{\Theta}_T^t\boldsymbol{\Theta}_T$ are in $\left[(1-\delta_K)^2, (1+\delta_K)^2\right]$ [12]. Moreover, RIP of order K implies that RIP holds for sparsity less than K as well. It is important to note that the RIP is predominantly used to establish theoretical performance guarantees when either the measurement vector **y** is corrupted with noise or the vector **x** is not strictly K-sparse.

2.6 CS for FSK modulated signals

We consider that the N×1 vector **s** represents the FSK modulated signal transmitted in the time domain. As the FSK signal **s** is sparse in frequency domain, it can be expressed by the product of the N×N basis matrix **B** and the sparse coefficient N×1 vector **a**, like

$$\mathbf{s} = \mathbf{B}\mathbf{a} \tag{2.17}$$

where **B** is equal with the normalized inverse discrete Fourier transform (IDFT) matrix $\mathbf{F}^H$, and each element of **a** corresponds to a carrier frequency. If **F** represents the N×N normalized discrete Fourier transform (DFT) matrix, then

$$\mathbf{F}^H = (\mathbf{F})^{-1} \tag{2.18}$$

is the normalized inverse discrete Fourier transform (IDFT) matrix, where $(.)^H$ stands for the Hermitian matrix of **F**, so that $\mathbf{F}^H\mathbf{F} = \mathbf{I}$. The non-zero components of $\mathbf{a}_{N\times1}$ represent the active carriers. So, equation (2.17) can also be written as

$$\mathbf{s} = \mathbf{F}^{H}\mathbf{a}. \tag{2.19}$$

The transmitted signal passes through the communication channel, and additive white Gaussian noise (AWGN) is added to the signal. When the signal arrives at the receiver has the form

$$\mathbf{x} = \mathbf{H}\mathbf{F}^{H}\mathbf{a} + \mathbf{n} \tag{2.20}$$

where $\mathbf{H}_{N\times N}$ denotes the channel convolution matrix and $\mathbf{n}_{N\times 1}$ the noise vector. Subsequently, in order to reduce the complexity and sampling rate at the receiver, we compress the received signal and then estimate the original one from fewer linear measurements. Since the signal x is sparse in frequency domain, it can be represented by M linear measurements with $M \ll N$. After compressed sensing, we can write the received signal as

$$\mathbf{y} = \mathbf{\Phi}\mathbf{x} \tag{2.21}$$

or as,

$$\mathbf{y} = \mathbf{\Phi}\mathbf{H}\mathbf{F}^{H}\mathbf{a} + \mathbf{\Phi}\mathbf{n} \tag{2.22}$$

where $\mathbf{\Phi}_{M\times N}$ is the transform operator or measurement matrix with M functionals as its rows, and $\mathbf{y}_{M\times 1}$ the compressed signal vector. As measurement matrix, we define M rows from the M×N IDFT matrix. In figure 2.6 for instance, it can be seen how the sparse vector $\mathbf{x}_{8\times 1}$ can be expressed in reduced dimensions of vector $\mathbf{y}_{4\times 1}$, after its product computation with matrix $\mathbf{\Phi}_{4\times 8}$.

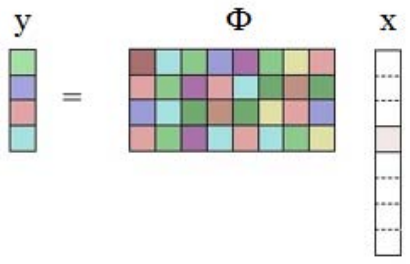

Figure 2.6: Matrix representation for the CS model $\mathbf{y} = \mathbf{\Phi}\mathbf{x}$.

By using the equation $\mathbf{F}^{H}\mathbf{F} = \mathbf{I}$, we can write equation (2.22) as,

$$\mathbf{y} = \Phi\mathbf{F}^{H}\mathbf{D}\mathbf{a} + \Phi\mathbf{n} \tag{2.23}$$

with the N×N matrix $\mathbf{D} := \mathbf{F}\mathbf{H}\mathbf{F}^{H}$. In terms of our model equations (2.14) and (2.15), we can transform equation (2.23) as,

$$\mathbf{y} = \Phi\Psi\mathbf{s} + \Phi\mathbf{n} \tag{2.24}$$

where $\Psi = \mathbf{F}^{H}$ and $\mathbf{s} = \mathbf{D}\mathbf{a}$.

2.7 Signal Reconstruction

After the compressed sensing operation and before the final detection of the signal at the demodulator side, the compressed signal is being reconstructed. We tested and compared in our simulations two CS reconstruction algorithms, the Basis Pursuit (BP) and Orthogonal Matching Pursuit (OMP).

2.7.1 Basis Pursuit

Basis pursuit is an optimization problem of finding a minimum l_1-norm solution to an underdetermined linear system, likewise the one that we have as a result of the compressed sensing operation. Our underdetermined system as we have seen in equation (2.21) has the form

$$\mathbf{y} = \Phi\mathbf{x}$$

where Φ is the M×N sensing matrix, $\mathbf{y}$ is a vector of length M, and $\mathbf{x}$ a vector of length N, where $M \ll N$. It can be observed that the system has more unknowns than equations. Assuming that the matrix $\Phi\Phi^{H}$ is invertible, the system then will have infinitely many solutions. Basis Pursuit is based on the idea of minimizing the sum of absolute values of $\mathbf{x}$, namely, to solve the optimization problem:

$$\begin{aligned} &\arg\min_{\mathbf{x}} \|\mathbf{x}\|_1 \\ &\text{such that } \mathbf{y} = \Phi\mathbf{x} \end{aligned} \tag{2.25}$$

where $\|\mathbf{x}\|_1$ is the l_1 norm of $\mathbf{x}$, defined as

$$\|\mathbf{x}\|_1 := \sum_{n=0}^{N-1} |x(n)|. \tag{2.26}$$

The solution of Basis Pursuit can be found by solving traditional linear programming techniques whose computational complexities are polynomial in N. To obtain the solution we used the iterative "Split Augmented Lagrangian Shrinkage Algorithm", known as SALSA, which is very efficient with high-speed performance, especially for l_1 norm-based algorithms. In the following section is described in more detail the SALSA algorithm and its particular application in signal reconstruction.

2.7.1.1 SALSA algorithm

SALSA is an iterative optimization algorithm based on the idea that combining the "augmented Lagrangian" approach and the "variable splitting technique," will lead to an effective algorithmic approach for solving linear inverse problems with sparse regularization. SALSA algorithm is known for its flexibility in handling various problems and its high convergence speed among all existing l_1 norm-based algorithms. The fast convergence is achieved using an alternating direction method of multipliers (ADMM), which is based on the augmented Lagrangian method (ALM) [9].

SALSA is used to obtain a solution to the basis pursuit problem for the efficient signal reconstruction. Basis pursuit as has been aforementioned picks the one sparse solution, the coefficients of which have a minimum l_1 norm, among the many possible solutions to $\mathbf{y} = \mathbf{\Phi x}$, and has the following form:

$$\mathbf{x}^{opt} = \arg\min_{\mathbf{x}} \|\mathbf{x}\|_1 \quad \text{such that } \mathbf{y} = \mathbf{\Phi x} \tag{2.27}$$

where $\mathbf{x}$ is the N×1 solution vector, $\mathbf{y}$ is the M×1 vector of observations and $\mathbf{\Phi}$ is a M×N measurement matrix with $M \ll N$.

SALSA is mainly based on the method of Augmented Lagrangian, which for the constraint optimization problem,

$$\arg\min_{z} E(\mathbf{z}) \quad \text{such that } \mathbf{Cz} - \mathbf{b} = 0, \tag{2.28}$$

is defined as

$$L_A(\mathbf{z},\mathbf{a},\mu) = E(\mathbf{z}) + \mathbf{a}^T(\mathbf{C}\mathbf{z}-\mathbf{b}) + \mu\left\|\mathbf{C}\mathbf{z}-\mathbf{b}\right\|_2^2 \tag{2.29}$$

In equation (2.29) the vector, **a**, are Lagrange multipliers. Augmented Lagrangian Method (ALM) for solving the constrained problem is given by the following operations which are iterated until convergence after the definition of variables $\mu > 0$ and vector **d**.

$$\mathbf{z} \leftarrow \arg\min_{z} E(\mathbf{z}) + \mu\left\|\mathbf{C}\mathbf{z}-\mathbf{b}\right\|_2^2 \tag{2.30a}$$

$$\mathbf{d} \leftarrow \mathbf{d} - (\mathbf{C}\mathbf{z}-\mathbf{b}) \tag{2.30b}$$

This method is also known as the method of multipliers (MM), so this iterative algorithm is referred to as ALM/MM in [11]. The ALM/MM algorithm calls for a positive scalar μ, which is like a step-size parameter. Its value can affect the convergence speed of the algorithm, but not the solution to which it converges. The vector **d** is initialized before the iteration and usually with a value equal to zero.

2.7.1.2 SALSA for Basis Pursuit

More precisely, the implementation of SALSA algorithm for solving the problem of basis pursuit is formulated as below. First of all, by using the variable splitting technique, the classical expression of basis pursuit

$$\mathbf{x}^{opt} = \arg\min_{\mathbf{x}} \left\|\boldsymbol{\lambda} \odot \mathbf{x}\right\|_1 \quad \text{such that } \mathbf{y} = \boldsymbol{\Phi}\mathbf{x} \tag{2.31}$$

can be transformed to an equivalent optimization problem

$$x^{\mathbf{opt}} = \arg\min_{\mathbf{x}} \left\|\boldsymbol{\lambda} \odot \mathbf{u}\right\|_1 \quad \text{such that } \mathbf{y} = \boldsymbol{\Phi}\mathbf{x},\ \mathbf{u} - \mathbf{x} = 0, \tag{2.32}$$

where the $\odot$ operator denotes the element-wise multiplication. For instance, for the equal-size vectors $\boldsymbol{\lambda}$ and **u**, it is, $[\lambda \odot u]_i = \lambda_i u_i$ while when all elements of vector $\boldsymbol{\lambda}$ are the same value, (i.e. $\lambda_i = \lambda \in R_+$), then equation (2.32) can be written as

$$\mathbf{x}^{\text{opt}} = \arg\min_{x} \boldsymbol{\lambda} \|\mathbf{u}\|_1 \quad (2.33)$$
$$\text{such that } \mathbf{y} = \boldsymbol{\Phi}\mathbf{x}$$
$$\mathbf{u} - \mathbf{x} = 0 .$$

Subsequently, by using the augmented Lagrangian expression

$$L_A(\mathbf{x}, \mathbf{u}, \boldsymbol{\lambda}, \mu) = \|\boldsymbol{\lambda} \odot \mathbf{u}\|_1 + \boldsymbol{\lambda}^T (\mathbf{u} - \mathbf{x}) + 0.5\mu \|\mathbf{u} - \mathbf{x}\|_2^2 + \boldsymbol{\lambda}_2 (\boldsymbol{\Phi}\mathbf{x} - \mathbf{y}), \quad (2.34)$$

as well as the ALM/MM to solve the problem, the algorithm obtains the following form:

Step 1: initialize the variables $\mu > 0$, $\mathbf{d}$
Step 2: iteration until convergence

$$x, u \leftarrow \begin{cases} \arg\min_{x,u} \|\boldsymbol{\lambda} \odot u\|_1 + 0.5\boldsymbol{\mu} \|u - x - d\|_2^2 \\ \text{such that } \mathbf{y} = \boldsymbol{\Phi}\mathbf{x} \end{cases} \quad (2.35a)$$

$$\mathbf{d} \leftarrow \mathbf{d} - (\mathbf{u} - \mathbf{x}) \quad (2.35b)$$

At this point, a technique known as Alternating Direction Method of Multipliers (ADMM), states that if the minimization is performed alternately between two vectors, like in expression (2.35a) between **x** and **u**, then the algorithm will still converge to the global minimum[9]. Taking into consideration this method and by alternating between minimization with respect to each of **x** and **u**, we get the following form of the algorithm:

Step 1: initialize the variables $\mu > 0$, $\mathbf{d}$
Step 2: iteration until convergence

$$\mathbf{u} \leftarrow \arg\min_{u} \|\boldsymbol{\lambda} \odot \mathbf{u}\|_1 + 0.5\mu \|\mathbf{u} - \mathbf{x} - \mathbf{d}\|_2^2 \quad (2.36a)$$

$$\mathbf{x} \leftarrow \begin{cases} \arg\min_{x} \|\mathbf{u} - \mathbf{x} - \mathbf{d}\|_2^2 \\ \text{such that } \mathbf{y} = \boldsymbol{\Phi}\mathbf{x} \end{cases} \quad (2.36b)$$

$$\mathbf{d} \leftarrow \mathbf{d} - (\mathbf{u} - \mathbf{x}) \quad (2.36c)$$

The minimization with respect to **u** in equation (2.36a) can be expressed in terms of "soft-thresholding".

Soft-thresholding is a popular tool which allows us to find an efficient solution in a fast way (or low computation time) and usually has application in l_1 penalties. The function soft: $\mathbb{C} \times \mathbb{R}_+ \to \mathbb{C}$ is defined as Soft(x, T) = max(1-T/|x|,0) · x.

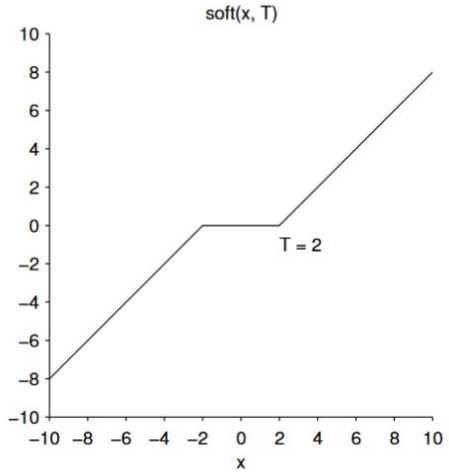

Figure 2.7: The soft-threshold function in real time [9].

With regards to minimization of **x**, which is a constrained least squares problem, there is a distinct solution in terms of matrix inverses. By exploiting these alternative solutions to each of the two minimization problems, the algorithm transforms to:

Step 1: initialize the variables $\mu > 0$, **d**
Step 2: iteration until convergence

$$\mathbf{u} \leftarrow \text{soft}(\mathbf{x} + \mathbf{d}, \lambda / \mu) \tag{2.37a}$$

$$\mathbf{x} \leftarrow (\mathbf{u} - \mathbf{d}) + \Phi^{H}\left(\Phi\Phi^{H}\right)^{-1}(\mathbf{y} - \Phi(\mathbf{u} - \mathbf{d})) \tag{2.37b}$$

$$\mathbf{d} \leftarrow \mathbf{d} - (\mathbf{u} - \mathbf{x}) \tag{2.37c}$$

With a substitution of $\mathbf{v} = \mathbf{u} - \mathbf{d}$, the arithmetic operations in iteration can be reduced as below:

$$\mathbf{v} \leftarrow \text{soft}(\mathbf{x} + \mathbf{d}, \lambda / \mu) - \mathbf{d} \tag{2.38a}$$

$$\mathbf{x} \leftarrow \mathbf{v} + \Phi^{H}\left(\Phi\Phi^{H}\right)^{-1}(\mathbf{y} - \Phi\mathbf{v}) \tag{2.38b}$$

$$\mathbf{d} \leftarrow \mathbf{x} - \mathbf{v} \tag{2.38c}$$

The algorithm can be further simplified by a slight rearrangement of operations:

Step 1: initialize the variables $\mu > 0$, **d**
Step 2: iteration until convergence

$$\mathbf{v} \leftarrow \text{soft}(\mathbf{x} + \mathbf{d}, \lambda / \mu) - \mathbf{d} \tag{2.39a}$$

$$\mathbf{d} \leftarrow \Phi^{H}\left(\Phi\Phi^{H}\right)^{-1}(\mathbf{y} - \Phi\mathbf{v}) \tag{2.39b}$$

$$\mathbf{x} \leftarrow \mathbf{d} + \mathbf{v} \tag{2.39c}$$

It could be noted that at every iteration, **x** satisfies **Φx** = **y**. This is because,

$$\begin{aligned}\Phi(\mathbf{d}+\mathbf{v}) &= \Phi\left[\Phi\left(\Phi\Phi^{H}\right)^{-1}(\mathbf{y}-\Phi\mathbf{v})+\mathbf{v}\right] \\ &= \Phi\Phi^{H}\left(\Phi\Phi^{H}\right)^{-1}(\mathbf{y}-\Phi\mathbf{v})+\Phi\mathbf{v} \\ &= (\mathbf{y}-\Phi\mathbf{v})+\Phi\mathbf{v} \\ &= \mathbf{y}. \end{aligned} \tag{2.40}$$

In our implementation, matrix **Φ** is the inverse N-point DFT matrix, and due to the orthogonality properties of complex sinusoids, this matrix satisfies $\Phi\Phi^{H} = p\mathbf{I},\ p > 0$.

As a result, SALSA algorithm for solving the Basis Pursuit problem takes the final form:

Step 1: initialize the variables $\mu > 0$, **d**
Step 2: iteration until convergence

$$\mathbf{v} \leftarrow \text{soft}(\mathbf{x}+\mathbf{d}, \lambda/\mu) - \mathbf{d} \tag{2.41a}$$

$$\mathbf{d} \leftarrow \frac{1}{p}\Phi^{H}(\mathbf{y}-\Phi\mathbf{v}) \tag{2.41b}$$

$$\mathbf{x} \leftarrow \mathbf{d}+\mathbf{v} \tag{2.41c}$$

2.7.2 Orthogonal Matching Pursuit (OMP)

Orthogonal Matching Pursuit (OMP) is an alternative algorithm for signal reconstruction having as a major advantage the low computational complexity and the opportunity for simple and fast implementation. Especially when the signal vector is highly sparse, the computational cost and time seem to have better results, compared to the Basis Pursuit. We use the OMP algorithm for recovery of the K-sparse signal **x** under the model **y** = **Φx**. The aim is to identify the location of the basis vectors in **Φ** which represent ideally the received signal **x**. The columns can be determined by projecting the signal onto its measurement matrix **Φ**. More specifically, OMP is an iterative greedy algorithm that selects at each step the column of **Φ** which is most correlated with the current residuals. The column is then added to the set of the already selected columns. One of the most important properties of the algorithm is that the same atom is not chosen twice. The residuals are being updated by projecting the observation onto the linear subspace spanned by the columns that have already been selected, and then the algorithm continues to iterate a number of times as per requirement for the algorithm to converge.

In our case, the measurement matrix $\mathbf{\Phi}_{M\times N}$ is the IDFT matrix and the M×1 dimensional column vectors $\boldsymbol{\varphi}_i$, where i = 1, 2, 3, …, N, constitute the matrix $\mathbf{\Phi}$. So it is

$$\mathbf{\Phi} = [\boldsymbol{\varphi}_1\ \boldsymbol{\varphi}_2\ \boldsymbol{\varphi}_3 \dots\ \boldsymbol{\varphi}_N].$$

Let Ω be the set of vectors which are more correlated with the signal and can represent it in the best way. At each iteration, the set will have a new index of the suitable vector with the most correlated column. In addition, Ω is an empty set at the time of initialization, i.e., $\Omega_0 = \{\emptyset\}$. The steps involved in the implementation of the reconstruction algorithm OMP are the following:

Step 1: Initialize the set $\Omega_0 = \{\emptyset\}$ and the residual equal with the received signal **y**;
$\mathbf{r_0} = \mathbf{y}$.

Step 2: At the k-th iteration, $\mathbf{r}_k$ is projected onto all columns of $\mathbf{\Phi}$ and the value which is most correlated is selected for the set Λ;

$$\mathbf{c}_{k+1} = \max\left|\left\langle \mathbf{r}_k, \boldsymbol{\varphi}_i \right\rangle\right| : i = 1,\ 2,\ 3,\ \dots,\ N-k, \tag{2.42}$$

and let,

$$\Lambda_{k+1} = \{i : \left|\left\langle \mathbf{r}_{k,}, \boldsymbol{\varphi}_i \right\rangle\right| \geq a\mathbf{c}_{k+1} :\ i = 1,\ 2,\ 3,\ \dots,\ N-k \text{ and } 0 < a < 1\}, \tag{2.43}$$

where the set Λ_{k+1} contains the indices of the candidate basis vectors.

Step 3: Among the vectors in the set Λ, the most appropriate vector seems to be the one which gives the minimum residual after being projected upon by the current residual, taking into consideration also the already most suitable selected vectors Ω_k.

$$\boldsymbol{\lambda}_{k+1} = \arg\min_{\lambda\in\Lambda}\left\{\left\|\mathbf{r}_k - P_{\text{span}\{\Phi_t\cup\lambda:t\in\Omega_k\}}\mathbf{r}\right\|_2\right\}, \tag{2.44}$$

Where the projection onto the linear space spanned by the elements of Ω_k is defined as

$$P_{\text{span}\{\theta_t\cup\lambda:t\in\Omega_k\}} = \Omega_k\left(\Omega_k{}^T\Omega_k\right)^{-1}\Omega_k{}^T \tag{2.45}$$

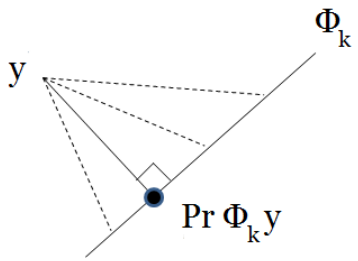

Figure 2.8: Geometry scheme of Projection.

Step 4: Then there is a union operation between the vector λ_{k+1} with the set of Ω_k;

$$\Omega_{k+1} = \Omega_k \cup \lambda_{k+1} \tag{2.46}$$

Step 5: The residual is updated;

$$\mathbf{r}_{k+1} = \mathbf{y} - P_{span\{\Phi_t : t \in \Omega_{k+1}\}}\mathbf{y} \tag{2.47}$$

The iteration continues until a certain level of residual error or until a maximum number of allowed iterations is achieved.

2.8 Signal Detection

Signal detection or demodulation is the procedure of extracting the original information content from the modulated carrier wave that is transmitted. When the signal passes through the communication channel, noise obscures and reduces the clarity of the signal to a great extent. For the proposed system, FSK demodulator is able to determine which of the two possible frequencies, representing transmission data bits 0 and 1, is present at a given time point, despite the presence of noise.

The FSK demodulator is CS-based, in the sense that before the final decision for which of the waveforms appear in the transmitted sequence, each one of them is being compressed so as to be estimated from fewer samples at reduced Nyquist rate. The signal estimation is then applied over the sub-sampled signal, which is being recovered using the CS reconstruction algorithms of BP or OMP.

Coherent FSK is the chosen demodulation scheme. The receiver by knowing the two prototype FSK modulated waveforms decides in favor of the one which is closest in Euclidean distance to the received noisy signal, in frequency domain. The decision about each waveform appearing in the received sequence is based on the minimum Euclidean distance between the DFT of the received reconstructed part of the signal after the CS

operation and the DFT two possible carrier waves that have been passed from the transmitter. The observed signal is defined as

$$\hat{\mathbf{s}} = \text{argmin}_{\mathbf{s}_i} \|\mathbf{c} - \mathbf{s}_i\|^2 \tag{2.48}$$

where **c** is the DFT vector of the received signal and $\mathbf{s}_i$ stands for the DFT of the two possible carrier waves $a_0(t) = A\cos(\omega_0 t + \theta_c)$ and $a_1(t) = A\cos(\omega_0 t + \theta_c)$, representing the binary data 0 and 1 respectively. In the end, the combination of detection and demodulation leads to the analog-to-digital conversion of the signal, in terms of mapping

continuous waveform $\widehat{x(t)} \rightarrow \hat{m}$ discrete message.

The analog to digital conversion process produces sequences of binary numbers that represent the observed analog data at particular regular points. In Figure 2.9 is illustrated in detail the whole proposed communication system model.

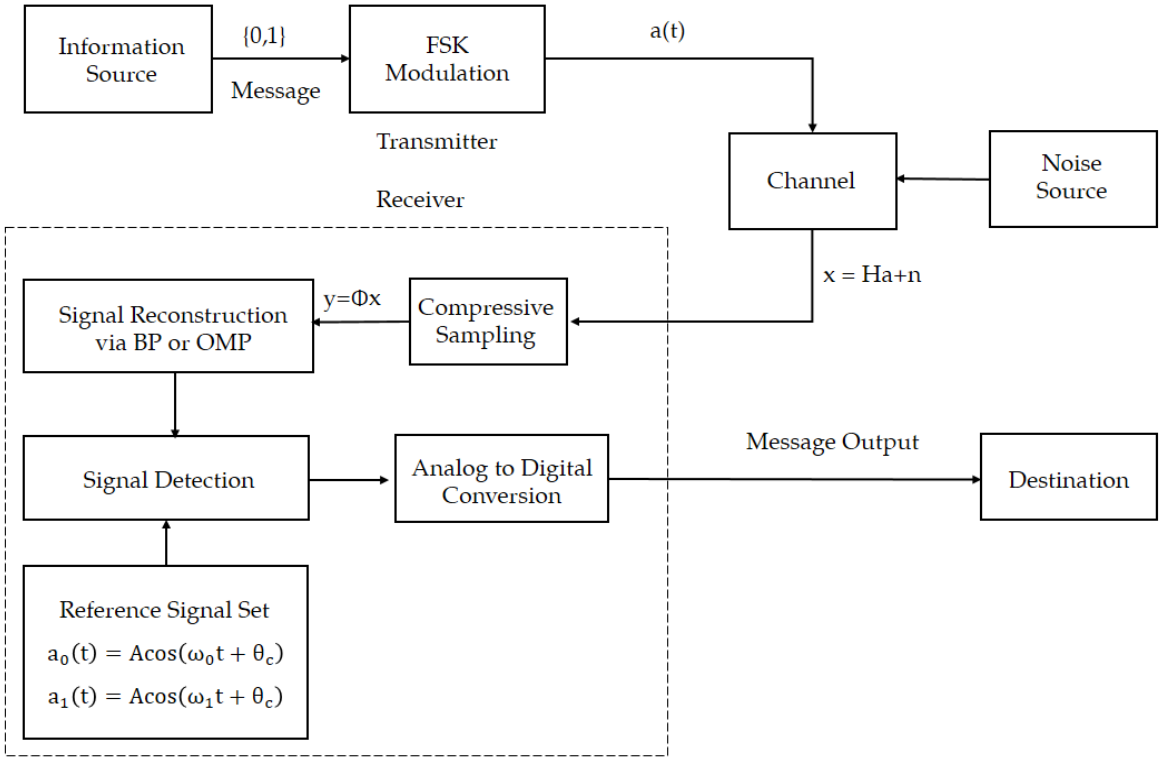

Figure 2.9: Block diagram of the proposed System Model.

Chapter 3
Simulation and Results

3.1 Simulation Approach

After successfully developing the software of all the blocks of the proposed system model illustrated in Figure 2.9 in MatLab (Matrix Laboratory) environment, simulations have been conducted so as to estimate the efficiency of the system. We evaluate their performance initially through simulations in AWGN channel and then in space channel model, being able in that way to compare and estimate whether the FSK modulator and FSK CS-based demodulator pair would be effective in applications of space communications despite the non-favorable communication conditions in the space environment.

More precisely, the communication system consisting of the transmitter, the communication channel and the receiver, has been simulated as follows; as an initial step, a long sequence of random bits are being generated, which are being provided as input to the transmitter. At the transmitter, FSK modulation is applied in the input sequence, which is synthesized in terms of two waveforms with specific frequencies as a reference, representing each one the binary bits 0 and 1. The modulated carrier signal in analog form is then transmitted through the simulated channel. We tested the transmission performance of the signal through two separate channel models, in the AWGN channel, as well as in the space channel model. During the transmission, a controlled amount of noise is being added to the transmitted signal, which then becomes the input to the receiver. At the receiver side, the received signal is being compressed in the frequency domain, so as to be estimated then from fewer linear measurements, reducing in this way the sampling rate. The sub-sampled signal is being reconstructed through the CS recovery algorithms of BP and OMP, for the demodulation process. Finally, by computing the minimum value of the Euclidean distance between the frequency spectrum of the reconstructed signal and corresponding one of the prototype FSK waveforms, is specified the final sequence of the received message.

3.2 Simulation in AWGN Channel

Additive White Gaussian Noise (AWGN) channel is commonly used to simulate background noise of the channel under study. White Gaussian noise is normally distributed in time domain with zero mean and variance σ^2. In the following simulations we use it as a reference channel for the proposed communication system, the behavior of which we will compare next with its performance in the space channel model.

The performance results of the system based on FSK modulation and CS-based detection is presented in the plot of Figure 3.1. Evaluation of the performance is based on metrics of Bit Error Ratio (BER) and Signal-to-Noise Ratio (SNR).

BER indicates the number of bit errors divided by the total number of transmitted bits during a time interval. For each error that occurs means that the received bit is not equal with the transmitted one. Our goal is to provide a receiver in which the probability of errors is minimized for transmission in the simulated communication channels. SNR is defined as the ratio between the power of the signal and the power of background noise expressed in decibels (dB).

$$\mathrm{SNR} = \frac{P_{\mathrm{signal}}}{P_{\mathrm{noise}}} = \frac{E_b}{N_0} \tag{3.1}$$

In Figure 3.1 can be seen the performance of the FSK CS-based detector compared to the one in which the signal is being sampled at the Nyquist rate. More specifically, the Figure 3.1 shows four curves, where the two of them illustrate the CS-based demodulator which uses the BP and OMP as reconstruction algorithms, the third one the FSK detector without using CS operation, and the last one the theory BER of FSK detection.

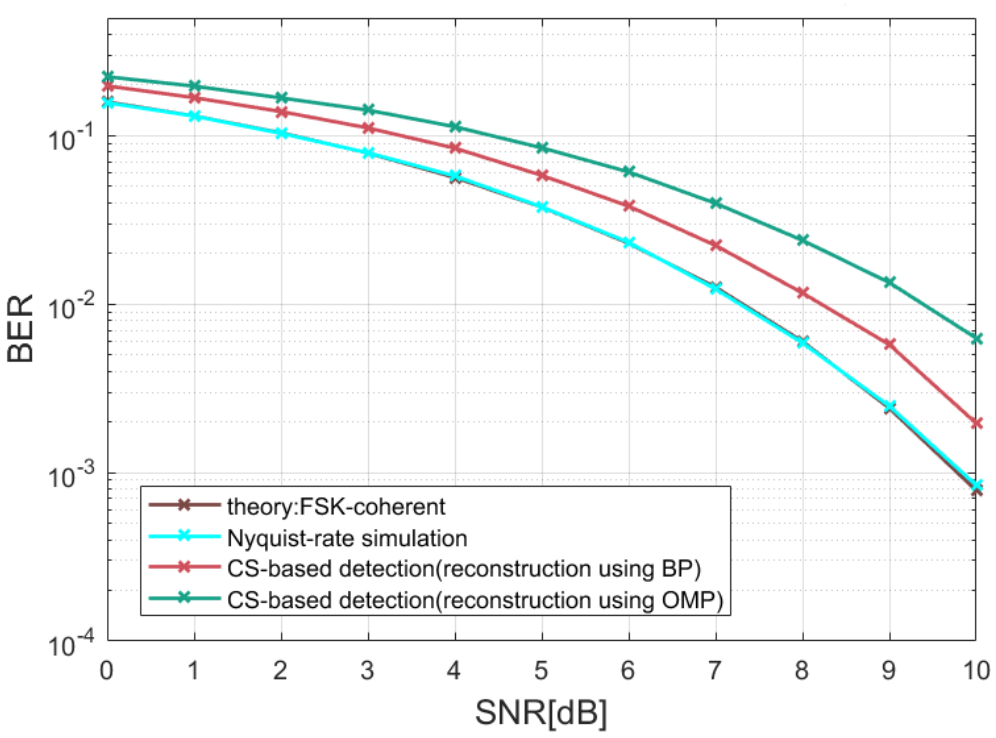

Figure 3.1: Average BER of FSK signal demodulation for CR = 0.8, AWGN channel, measurement matrix = IDFT matrix, reconstruction algorithms BP and OMP.

It can be observed that the theoretical curve is closely followed by the one that represents FSK detection at Nyquist-rate, while the latter appears better performance compared to the CS-based detectors. In this simulation for the CS-detectors, we assume a compression ratio of 0.8 (with M = 0.8N) per transmitted symbol, with the compression ratio (CR) measured as

$$CR = \frac{M}{N} \tag{3.2}$$

where M and N represent the compressed data size and the original data size (number of Nyquist-rate samples of an FSK symbol), respectively. As measurement matrix IDFT matrix is used. Furthermore, a coding gain up to 1 dB appears in the CS-based detection with reconstruction algorithm the BP, in comparison with the detection using OMP as recovery algorithm. For both the CS-based detections, the proposed system shows favorable results, as the SNR loss is not large compared with the one corresponding to the performance of demodulation without using Compressive Sampling technique. The overall results of the simulated detectors show a good Bit Error Rate performance, as the values of BER are close enough to the values of theory prediction for FSK detection, and moreover, there is a continuous drop in Bit Error values as the SNR increases.

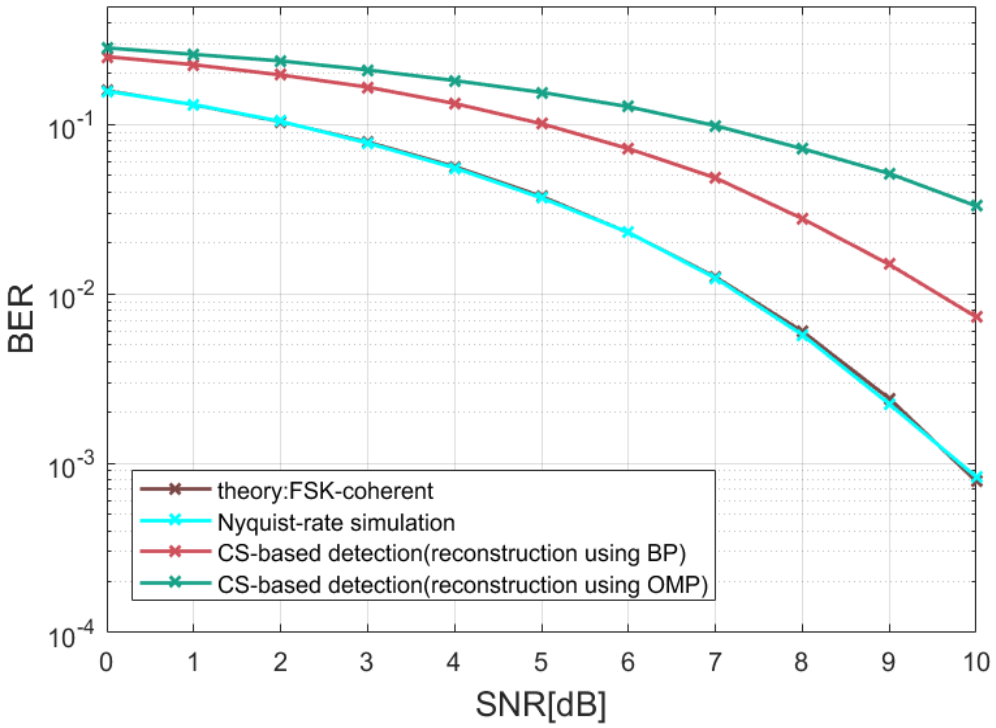

Figure 3.2: Average BER of FSK signal demodulation for CR = 0.6, AWGN channel, measurement matrix = IDFT matrix, reconstruction algorithms BP and OMP.

In the simulation of Figure 3.2 a compression ratio of 0.6 with M = 0.6N is applied, with measurement matrix the IDFT as well. We observe in general that as the sampling rate is being reduced, from 0.8 to 0.6, the Bit Error Rate for individual values of SNR is increased. Nonetheless, the difference between the plots with CS operation and the one without CS is around 2 and 3 dB, which is a good performance taking into consideration that the compression ratio is equal to 0.6.

In Figure 3.3 is represented simulation results for the probability of bit error as a function of compression ratio for SNR value of 10 dB. In this case, it is considered as N = 16 and M = 1:N, with measurement matrix the IDFT matrix. In the plot of Figure 3.3 the detection which is based on the reconstruction algorithm OMP shows better performance for compression ratio until 50%, while for larger compression ratios BP appears better BER performance.

However, the overall BER results of the both CS-based detectors are close enough to each other. It can also be observed that for a fixed value of SNR, as the number of samples per bit is rising, which means that the value of the relation M/N is increasing, then the probability of bit error appears a relatively steady drop. There are points where the BER values are increased for certain compressive ratios instead of having a continuous falling behavior. This behavior depends on the algorithms for signal reconstruction and the number of iterations they execute until convergence to obtain the final reconstructed signal.

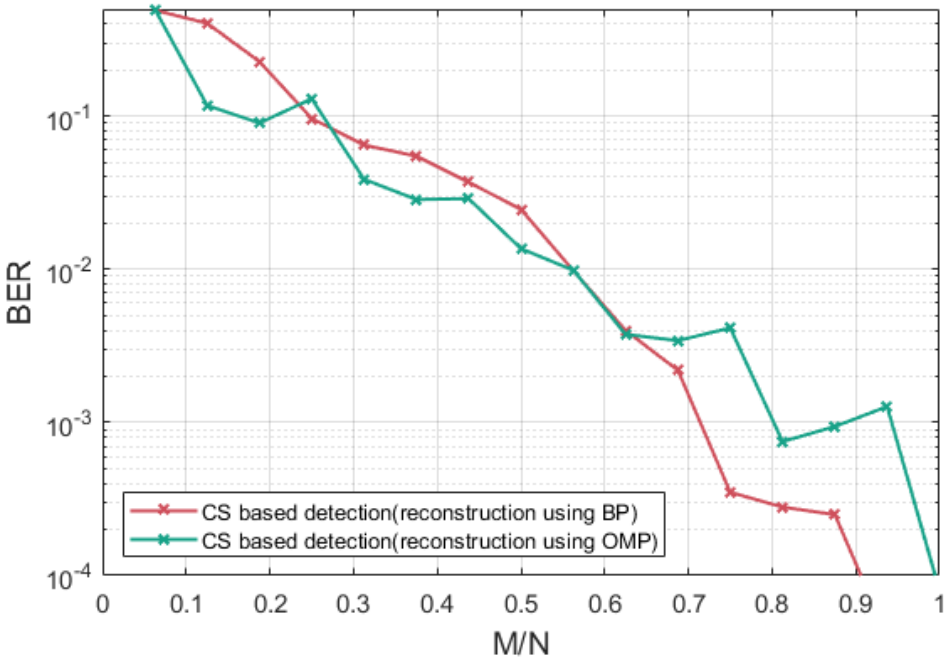

Figure 3.3: BER Vs Compression Ratio for 10 dB, AWGN channel, measurement matrix = IDFT matrix, N = 16, M = [1:N], reconstruction algorithms BP and OMP.

3.3 Simulation in Space Channel

We reveal the performance of the developed FSK modulation and CS-based demodulation schemes under the space channel model; a model introduced and implemented by HELIOS (Highly rEliable LInks during sOlar conjunctionS) project, an integrated project receiving funding from the European Space Agency (ESA) [1]. The space channel used is a Rician channel based on experimentally derived power spectral densities for the phase and amplitude of X-band signals propagating through the solar corona [1].

Rician fading is a stochastic model for radio propagation caused by the partial cancellation of a radio signal, and is typically used in space link communications, where the signal is strongly affected by amplitude and phase scintillation. We evaluate the performance of our implemented system through simulations in this Rician-based space channel, during periods of Solar Conjunction, when the Sun-Earth-Probe angle becomes extremely small reaching about 3º. The coherent sampling time is set equal to 0.1 seconds, while $K_r = 10$ is the Rician K-factor, denoting the ratio between the power in the direct path and the power in the scattered paths of the channel.

Figure 3.4 illustrates the performance of the Compressive Sampling-based demodulator for FSK modulated signals which are transmitted through the space communication link. More specifically, in Figure 3.4 are shown three curves, the two of them representing the CS-based demodulator which uses for signal reconstruction the BP and OMP algorithms, and a third one denoting the demodulator which samples at Nyquist-rate.

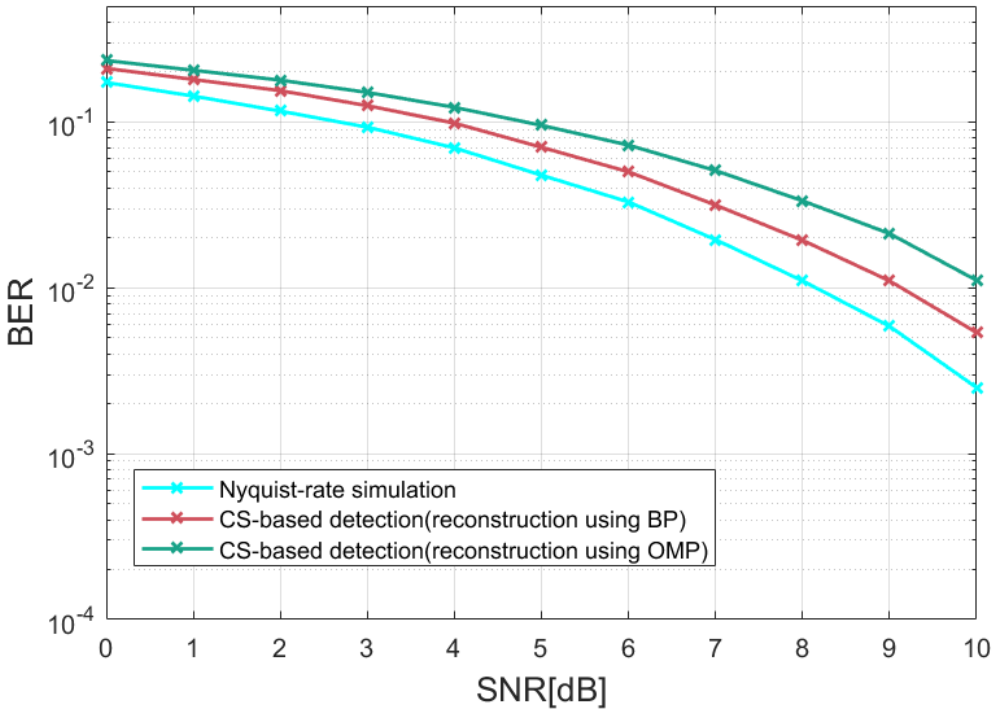

Figure 3.4: Average BER of FSK signal demodulation for CR = 0.8 in Space Channel, measurement matrix = IDFT matrix, reconstruction algorithms BP and OMP.

In the above simulation is considered a compression ratio of 0.8 (with M = 0.8N) per symbol transmitted through the space communication link, with the IDFT matrix as measurement matrix used. Although the optimum performance regarding BER-SNR is shown up from the detection based on Nyquist-rate sampling, Compressive Sampling-based detectors also appear a very effective performance under the space communication channel. As it can be observed, the curves representing the CS-based detectors reach Bit Error Rate close enough to the reference plot corresponding to demodulation of Nyquist-rate sampling.

More precisely, the simulation results for CR = 0.8 show a coding gain of 1 dB for the non-CS-based detector, compared with the CS-based one which uses BP as reconstruction algorithm, as well as a coding gain of 2 dB in comparison with demodulator using OMP as a recovery method.

In Figure 3.5 are illustrated the results of the Compressive Sampling-based demodulators, when there is applied a more strict Compression Ratio equal to 0.6. As it was expected, this drop of CR = 0.8 to CR = 0.6, leads to a relative increment in the values of Bit Error Rate. For instance, we observe that in case of CR = 0.6, for SNR = 5 dB, BER reaches values a little higher than 10^{-1} for the both CS-based detectors, while in the above simulation of CR = 0.8, is achieved a BER little less than 10^{-1} for SNR equal to 5 dB. Although the sampling rate is significantly reduced, the results confirm the efficiency of the proposed implemented system, as there is not large divergence between the BER values of the cases above in which are applied different compressive sampling ratios (in the first instance CR = 0.8, while in the second CR = 0.6). Furthermore, BER appears a stable downward behavior when the SNR values raise.

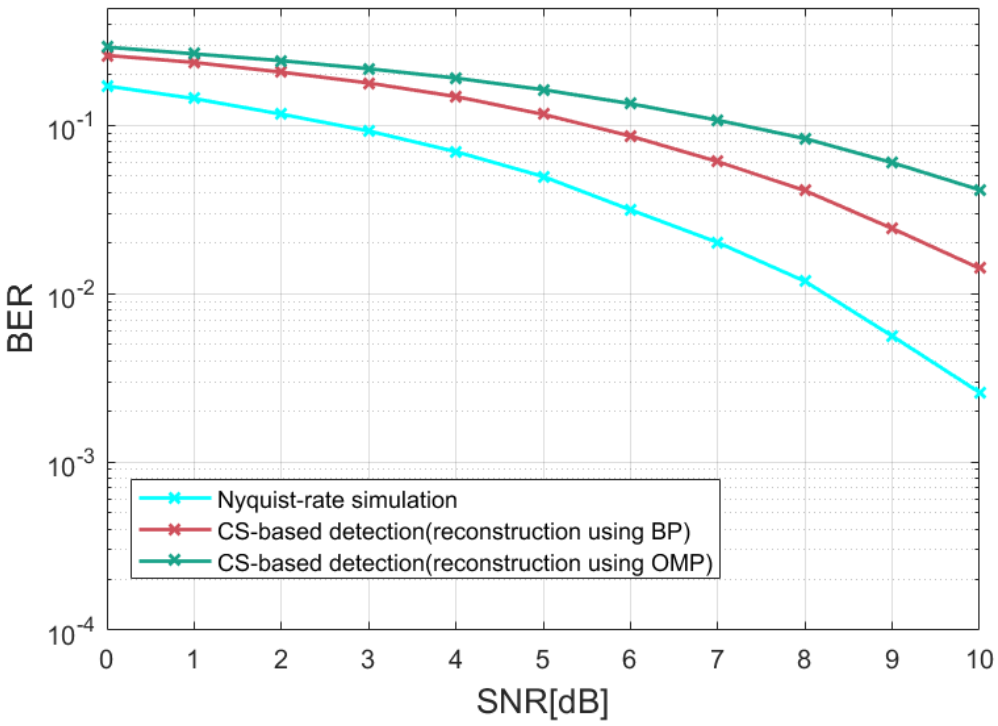

Figure 3.5: Average BER of FSK signal demodulation for CR = 0.6 in Space Channel, measurement matrix = IDFT matrix, reconstruction algorithms BP and OMP.

We tested furthermore the performance of the system not only for the instances presented in Figures 3.4 and 3.5, but also for more values of Compression Ratio which are greater and lower of the above. Our inference is that as the Compression Ratio declines further, the coding gain of the detector based on Nyquist rate sampling raises, but that is not to a large extent, if we take into consideration all the benefits of Compressive Sensing that results in a low-complexity hardware in the receiver of the communication system. The observations prove that Compressive Sensing could be efficiently used in practical space communication environments.

Figure 3.6 shows the simulation outcomes for the probability of bit error as a function of compression ratio, when the SNR equals to 10 dB. For this scenario, we considered N = 16, M = 1:N, and IDFT matrix as measurement matrix. The simulation has been conducted under the space channel model, the results of which show that in this case the overall performances of both CS-based demodulators using BP and OMP as reconstruction algorithms respectively, are sufficiently close to each other as the CR increases.

In addition, this simulation confirms the observation that as the compression ratio increases, the probability of bit error falls. In the CS plots of Figure 3.6 appear some fluctuations in values of BER, which can be attributed to the effect of each IDFT measurement matrix used in the 16 distinct Compressive Sampling simulated processes, represented by the points appearing in the plots. This behavior of BER fluctuations as the CR increases also depends on the reconstruction algorithms BP and OMP used, as well as on the number of iterations they execute until convergence to obtain the final reconstructed signal on which is based the final bit decision.

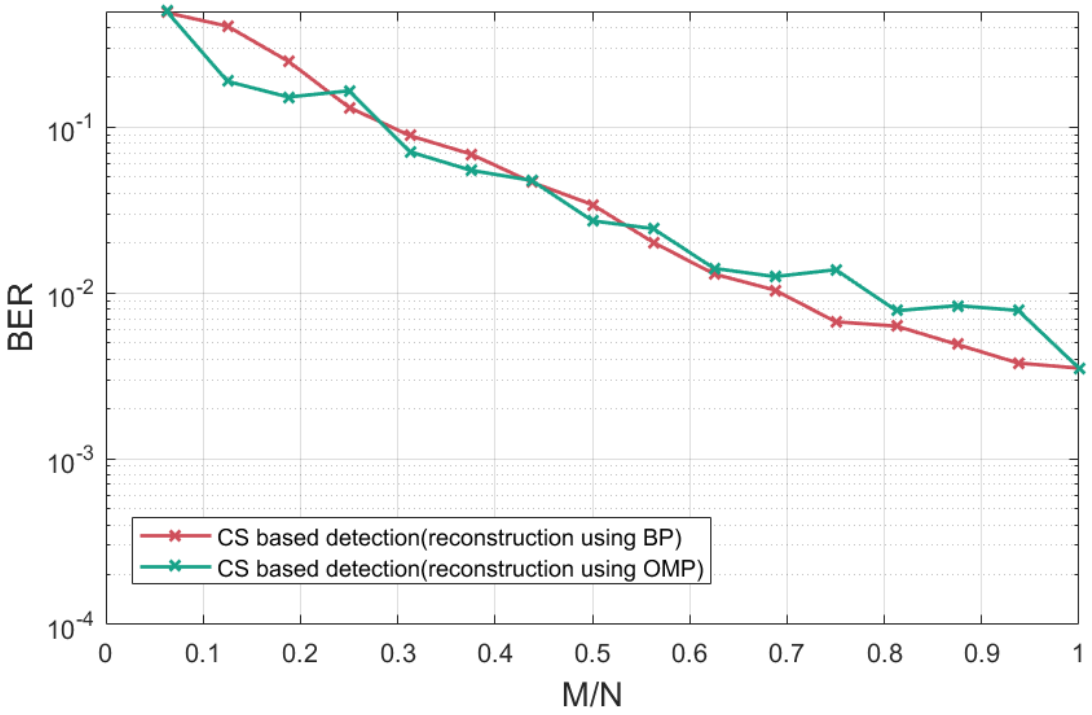

Figure 3.6: BER Vs Compression Ratio for 10 dB, Space Channel, measurement matrix = IDFT matrix, N = 16, M = [1:N], reconstruction algorithms BP and OMP.

Consequently, all the above simulation results of the implemented system model, prove the efficiency of Compressive Sampling-based techniques for FSK signals demodulation for transmission over the space communication link. Therefore, the proposed system would achieve a reliable communication between Earth and Space, being able to be also used in periods when communications face severe difficulties due to the hard conditions in the space environment.

Chapter 4
Conclusions and Future Work

Space link communications face severe challenges in a great extent, especially during periods of Solar Conjunction, when the angle between Sun-Earth and Probe appears a significant drop. The signal that is being transmitted under these conditions suffers from amplitude and phase scintillation, as well as from spectral broadening effects. Within this thesis, we focus on the study and development of Compressive Sampling-based techniques for FSK signals demodulation, exploring the performance of the system when the signals that are being transmitted through the space communication link have been altered, due to their passage through the solar corona.

Initially, all the essential theoretical background for the system's structure comprehension has been presented in detail, as well as the procedure that we followed for the development of the proposed system in MatLab environment. Afterwards, we evaluate the performance of the implemented scheme initially under the AWGN channel, and then under real Space channel assignment. The results demonstrate the effectiveness of the Compressive Sampling-based FSK demodulation scheme in space communications, as the Bit Error Rate shows low values in short SEP angles between the Spacecraft and the Earth. Compressive Sampling-based demodulation secures significant reduction in system's hardware complexity, power consumption and sampling rate at the receiver side of the communication system.

As a future research extension, Frequency-Hopping Spread Spectrum (FHSS) transmission through the Space communication link could be studied, in which the radio signals are being transmitted over rapidly changing frequencies, optimizing in that way the already implemented system. Furthermore, it could be studied alternative methods for compressed signals' reconstruction, which would ensure even better BER results and the overall system's optimum performance.

References

[1] A.J. Stocker, D.R. Siddle, E.M. Warrington, G. Mariotti, D. Silvestri, A. Zeqai, P. Tortora, A. Argyriou, J. De Vicente, R. Abello, and M. Mercolino, "A channel model for the propagation of X-band radio waves through the solar corona," URSI 2017.

[2] D. Morabito and R. Hastrup. "Communicating with Mars during periods of solar conjunction." In: IEEE Aerospace Conference Proceedings, pp. 1271- 1281, 2002.

[3] Q. Li, L. Yin and J. Lu. "Performance Study of a Deep Space Communications System with Low-Density Parity-Check Coding under Solar Scintillation." In: International Journal of Communications, Vol. 6(1), pp. 1-9.

[4] S. Gishkori, G. Leus and H. Deliç. "Energy detectors for sparse signals." In: Signal Processing Advances in Wireless Communications (SPAWC), IEEE Eleventh International Workshop, pp.1-5, 2010.

[5] I. Selesnick. "Introduction to Sparsity in Signal Processing." Connexions Website. http://cnx.org/content/m43545/, 2012.

[6] Watkins-Johnson Company. "FSK: Signals and Demodulation." Tech Notes. Vol.7(5), pp. 1-13, 1980.

[7] E.J. Candes and M.B. Wakin. "An Introduction To Compressive Sampling." In: IEEE Signal Processing Magazine, Vol. 25(2), pp. 21-30, 2008.

[8] M.M. Abo-Zahhad, A.I. Hussein, A.M. Mohamed "Compressive Sensing Algorithms for Signal Processing Applications: A Survey." In: International Journal of Communications, Network and System Sciences, Vol.8(6), pp. 197-216, 2015.

[9] I. Selesnick. L1-Norm Penalized Least Squares with SALSA. Connexions, 2014 http://cnx.org/content/m4893.

[10] T.T. Cai and L. Wang. "Orthogonal Matching Pursuit for Sparse Signal Recovery with Noise." In: IEEE Transactions on Information Theory Vol.57(7), pp. 4680-4688, 2011.

[11] M.V. Afonso, J.M. Bioucas-Dias and M.A.T. Figueiredo. "Fast image recovery using variable splitting and constrained optimization." In: Journal IEEE Transactions on Image Processing, Vol.19(9), pp. 2345-2356, 2010.

[12] A. Cohen, W. Dahmen, and R. DeVore, "Compressed sensing and best k-term approximation," preprint, pp. 1-23, 2006.